Supplementary

Unifying theories on the Southern Ocean bio-optical anomaly

Xuerong Sun*[1], Robert J. W. Brewin[1], Giorgio Dall'Olmo[2], Jaime Pitarch[3], Thomas G. Bell[4], Bethany Wilkinson[4], Dionysios E. Raitsos[5], Hendrik Jan van der Woerd[6], and Shubha Sathyendranath[4,7]

[1]Centre for Geography and Environmental Science, Department of Earth and Environmental Sciences, Faculty of Environment, Science and Economy, University of Exeter, Cornwall, United Kingdom

[2]Istituto Nazionale di Oceanografia e di Geofisica Sperimentale - OGS, Trieste, Italy

[3]National Research Council (CNR), Institute of Marine Sciences (ISMAR), Rome, Italy

[4]Plymouth Marine Laboratory, Plymouth, Devon, United Kingdom

[5]Department of Biology, National and Kapodistrian University of Athens, Athens, Greece

[6]Department of Water & Climate Risk, Institute for Environmental Studies (IVM), VU University Amsterdam, Amsterdam, the Netherlands

[7]National Centre for Earth Observation, Plymouth Marine Laboratory, Plymouth, Devon, United Kingdom

*Corresponding author: x.sun8@exeter.ac.uk

S1 Figures

S1.1 Figure S1

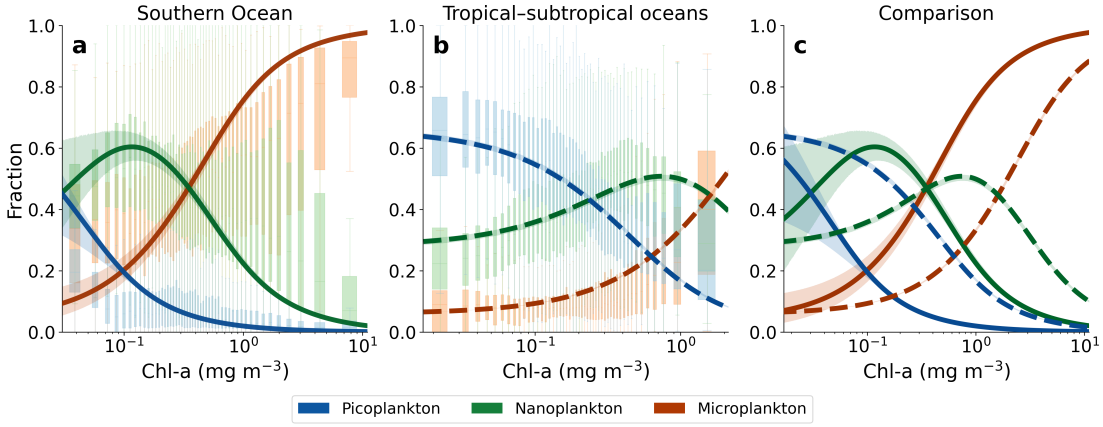

Figure S1. Same as Figure 2 in the main text. Given the large number of observations (16,977 Southern Ocean; 23,065 tropical-subtropical), individual dots overlap. Unlike Figure 2, which shows observation densities, here the in-situ measurements are summarised as box plots of the observed fractions (F_1, F_2, F_3) after $\log_{10}$-scale binning of Chl-a. Each box plot shows the median and interquartile range, with whiskers extending to 1.5×IQR. Bin widths vary on the raw Chl-a scale but have approximately equal sample counts.

S1.2 Figure S2

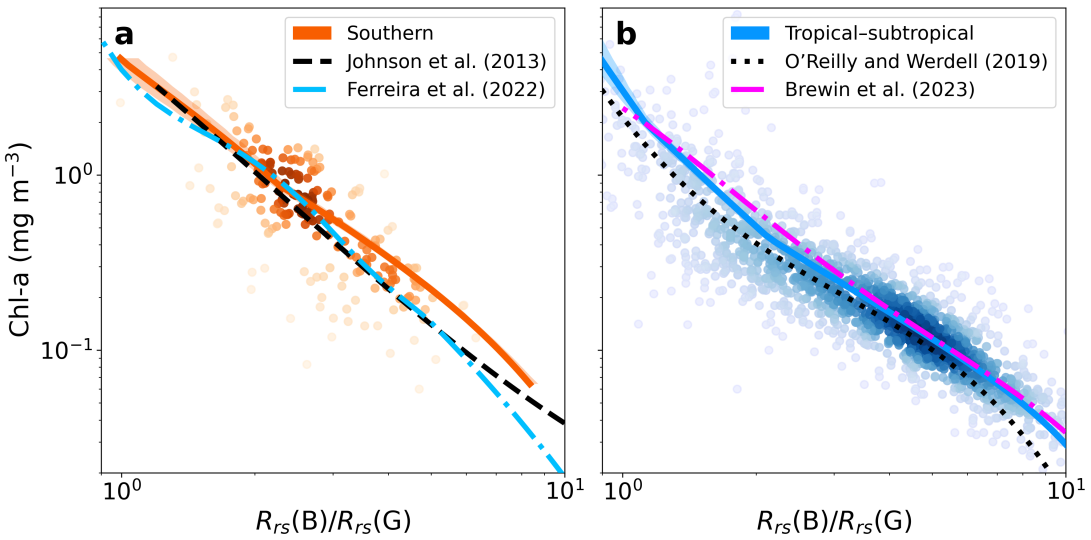

Figure S2. Ocean colour characteristics as a function of Chl-a across two ocean regions. a, Observations (dots) and model estimates (lines) of the relationship between the maximum blue-green band ratio (R_{rs}(B)/R_{rs}(G)) and Chl-a for the Southern Ocean, with relationships reported in previous studies (Johnson et al., 2013; Ferreira et al., 2022). b, Observations (dots) and model estimates (lines) of the relationship for the tropical–subtropical oceans, with previous results shown for comparison (O'Reilly and Werdell, 2019; Brewin et al., 2023).

S1.3 Figure S3

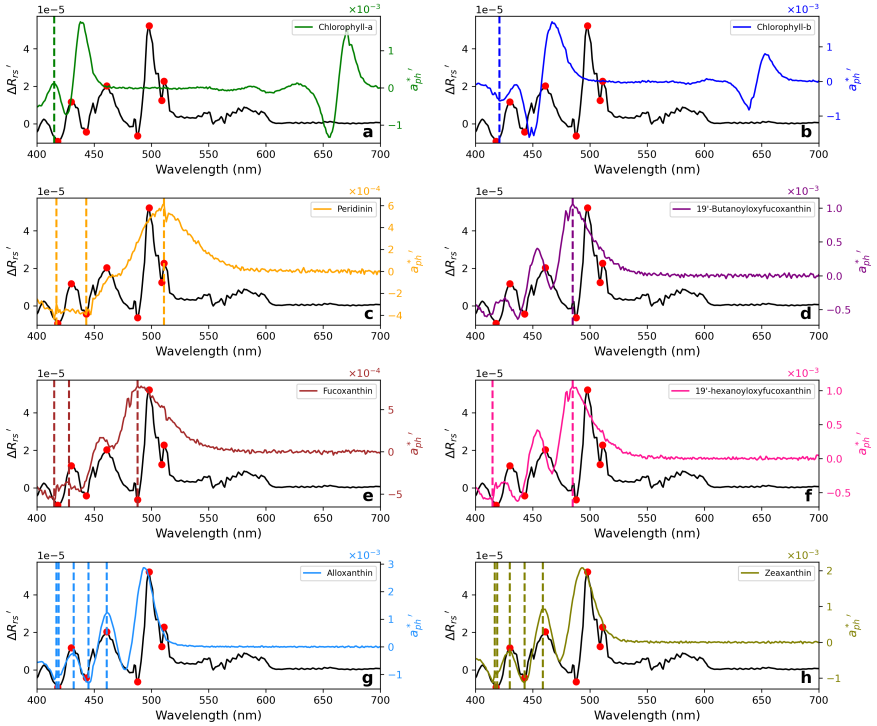

Figure S3. Comparison between the first derivative of hyperspectral remote sensing reflectance ($\Delta R_{rs}{}'$, black line, left y-axis) between the Southern Ocean and tropical–subtropical waters, and the first derivative of chlorophyll-specific absorption spectra ($a^*_{ph}{}'$, coloured line, right y-axis) for eight pigments (Clementson and Wojtasiewicz, 2019). Red circles indicate the prominent positions of peaks in $\Delta R_{rs}{}'$ (local maxima and minima), with vertical dashed lines representing pigment derivative peaks that fall within ±3 nm of these R_{rs} derivative features. Note that the spectra from Clementson and Wojtasiewicz (2019) were measured in solvent and differ from in-vivo absorption. They are used here as a reference for peak identification, while more direct comparisons would require in-vivo data.

A dataset of 10,000 simulated OCMF (Ocean Colour Modelling Framework) hyperspectral R_{rs} spectra was generated separately for the Southern Ocean and the tropical-subtropical regions. Chl-a were randomly sampled from a log-normal distribution (0.01 to 100 mg m^{-3}), with weighted sampling based on in-situ probability distributions to reflect regional variability. The difference in R_{rs}, ΔR_{rs}, was calculated as the median R_{rs} of the Southern Ocean minus that of the tropical–subtropical ocean. Its first derivative, $\Delta R_{rs}{}'$, was then computed, and peaks (local maxima and minima) were identified ('scipy.signal.find_peaks' in Python). To ensure robustness, bootstrap resampling (N = 1,000) was performed, and redundant peaks within ±1 nm of a more frequent peak were removed. Chlorophyll-specific absorption spectra (a^*_{ph}, m^2 (mg C)$^{-1}$) for eight phytoplankton pigments (Clementson and Wojtasiewicz, 2019) were interpolated to 1-nm resolution, and their first derivatives were compared to $\Delta R_{rs}{}'$.

The ΔR_{rs} spectrum exhibits eight prominent peaks at 418, 430, 443, 461, 488, 498, 509, and 511 nm. While some (e.g., 443 and 488 nm) align with bands of multispectral sensors, others (e.g., 418, 430, 461, 509, 511 nm) are unique to hyperspectral platforms, such as PACE, GLIMER, and HICO. By comparing the locations of $\Delta R_{rs}{}'$ peaks with those of $a^*_{ph}{}'$, we found that several features of R_{rs} differences are associated with specific pigments. For example, the 418 nm peak corresponds to multiple pigments, including alloxanthin, fucoxanthin, zeaxanthin, 19'-hexanoyloxyfucoxanthin, chlorophyll-a, and chlorophyll-b. Other peaks show more distinct associations. The 461 nm peak with alloxanthin and zeaxanthin, 489 nm with fucoxanthin, and 511 nm with peridinin, each serving as a diagnostic marker for certain phytoplankton groups.

S1.4 Figure S4

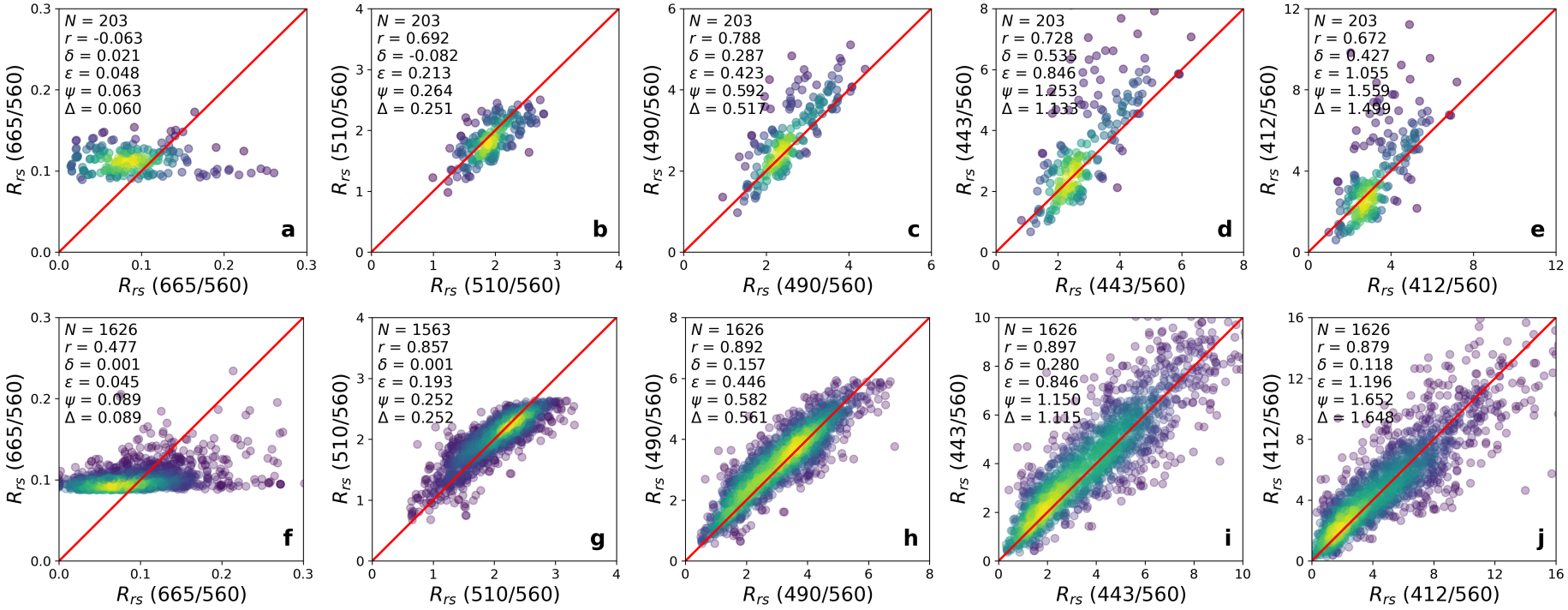

Figure S4. Independent validation of R_{rs} band ratios (normalised at 560 nm), comparing in-situ measurements (x-axis) with OCMF estimates (y-axis). a-e, Southern Ocean at 665, 510, 490, 443, and 412 nm; f-j, tropical–subtropical oceans at corresponding wavelengths. The red line indicates the 1:1 reference.

S2 In-situ Data

S2.1 HPLC pigments

This study compiled a dataset of 62,337 High Performance Liquid Chromatography (HPLC) samples collected from the global ocean. These include publicly available data from various sources, such as Australian Ocean Data Network (AODN, IMOS, 2021a,b), Biological and Chemical Oceanography Data Management Office (BCO-DMO, McGillicuddy, 2007b,a; DiTullio, 2011; Vaillancourt and Marra, 2011; Bidigare, 2012; Richardson et al., 2013; DiTullio, 2015; Lee, 2020; Lohrenz et al., 2020; Landry, 2021), DataONE (Palmer Station Antarctica LTER et al., 2020; Southern California Bight MBON et al., 2021), Environmental Data Initiative Data Portal (EDI, Palmer Station Antarctica LERT et al., 2018), NASA SeaWiFS Bio-optical Archive and Storage System (SeaBASS, Werdell et al., 2003), PANGAEA (Taylor et al., 2011b; Claustre, 2013; Bracher, 2014; Clayton et al., 2014; Peeken and Hoffmann, 2014; Peeken and Nachtigall, 2014; Bracher, 2015a; Bracher et al., 2015; Bracher, 2015b,c,d,e; Hepach et al., 2016; Peeken et al., 2017c,a,b; Peeken and Quack, 2017; Peeken and Walter, 2017; Peeken et al., 2017d; Taylor and Bracher, 2017; Bracher, 2019; Bracher et al., 2020; Xi et al., 2023), and some published works (Brewin et al., 2015; Jordan et al., 2024; Hayward et al., 2024).

To ensure data quality for subsequent analysis, several quality control steps were applied to the original HPLC dataset. When multiple samples were available at a station, each was treated as an individual observation. Each HPLC sample provides concentrations of total Chl-a (the sum of monovinyl chlorophyll-a, divinyl chlorophyll-a, and chlorophyllide-a) and seven diagnostic pigments used to infer phytoplankton size classes (Vidussi et al., 2001; Uitz et al., 2006). Samples with Chl-a below 0.001 mg m^{-3} were removed, and any diagnostic pigment values below this threshold were set to zero (Claustre et al., 2004). Additionally, samples were retained only if the difference between total chlorophyll concentration and total accessory pigments concentration did not exceed 30% of the total pigment concentration (Aiken et al., 2009). To maintain the independence of comparisons between Chl-a and blue-green R_{rs} band ratios, any HPLC samples with concurrent R_{rs} measurements were excluded. Since the Ocean Colour Modelling Framework (OCMF, see Section 4.4 in the main text for details) is designed for Case-1 waters, samples potentially from optically complex waters were removed using water type classifications derived from OC-CCI satellite data (see Section S3.2 for details). Samples was restricted to two regions of interest: the Southern Ocean (latitudes south of 60°S) and the combined tropical–subtropical oceans (between 40°N and 40°S). After applying all quality control and selection criteria, a total of 37,763 HPLC samples (N = 16,578 and 21,185 for the Southern Ocean and the tropical–

subtropical oceans, respectively) were retained for further analysis (Figure S5).

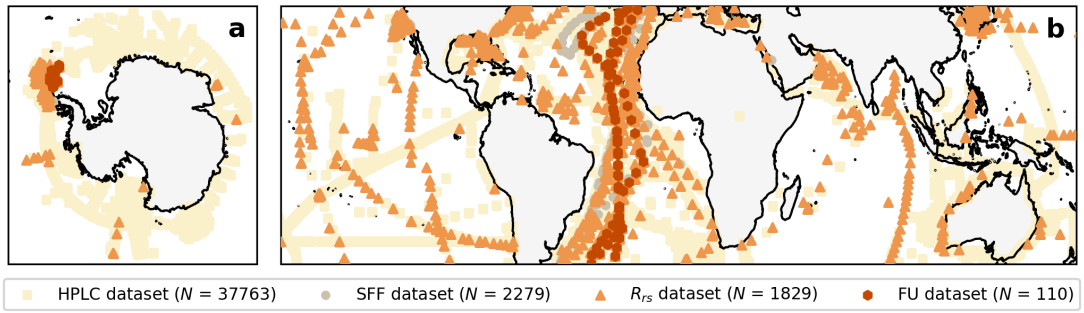

Figure S5. Geographic distribution of in-situ datasets used in this study for the Southern Ocean (south of 60°S, a) and tropical–subtropical regions (between 40°N and 40°S, b). Data include HPLC pigments (squares, N = 37,763), size-fractionated filtration (circles, N = 2,279), remote sensing reflectance (triangles, N = 1,829), and Forel-Ule colour observations (hexagons, N = 110).

S2.2 Size-fractionated filtration Chl-a

A total of 3,610 size-fractionated fluorometric (SFF) Chl-a measurements collected from the global ocean were used in this study. These include publicly available data from various sources, such as, British Oceanographic Data Centre (BODC, British Oceanographic Data Centre (BODC), 2020), DataONE (California Current Ecosystem LTER and Goericke, 2018; Sosik et al., 2021), and some published works (Brewin et al., 2014a, 2017, 2019; Venables et al., 2023).

In general, the Chl-a concentration in water passing through a 2 μm filter is designated C_1 (picoplankton), the concentration retained between the 2 and 20 μm filters as C_2 (nanoplankton), and the concentration retained on the 20 μm filter as C_3 (microplankton). The total Chl-a is calculated as the sum of these three size fractions. Following a quality control procedure similar to that applied to the HPLC dataset, samples with concurrent R_{rs} measurements or those potentially from optically complex coastal waters were excluded, resulting in 2,279 SFF samples remained for analysis, including 399 from the Southern Ocean and 1,880 from tropical–subtropical regions (Figure S5).

S2.3 Particulate absorption coefficients and Chl-a

From January to March 2024, we conducted a PICCOLO expedition (Processes Influencing Carbon Cycling: Observations of the Lower Limb of the Antarctic Overturning) in the Weddell Sea, Antarctica, one of the least-sampled regions of the Southern Ocean. One of the objectives of the cruise was to investigate the observed bio-optical anomaly.

During the cruise, particulate absorption coefficients ($a_p(\lambda)$), ranging from 400 to 750 nm, were measured quasi-continuously using an AC-S spectrophotometer (WET Labs, serial number 297). The AC-S was integrated into the underway optics system, following design and methods described in Dall'Olmo et al. (2009), which draws seawater from 7 m depth. The system collects concurrent measurements of total absorption and attenuation coefficients of the bulk water, $a(\lambda)$ and $c(\lambda)$, respectively. To distinguish particulate components, every hour the flow was automatically diverted for 10 minutes through a 0.2-μm filter (SUEZ Memtrex NY MNY921EGS), allowing computation of $a_p(\lambda)$ and particulate attenuation ($c_p(\lambda)$) by subtracting the filtered signal from the bulk. Data acquisition was initially managed by the WET Labs DH4 system and later transitioned to the open-source INLININO software (`https://github.com/OceanOptics/Inlinino`).

Post-processing included 1-minute binning, quality screening, and corrections for temperature and scattering effects. During binning, data affected by bubbles or flow blockages (e.g., from sea ice) were removed. Flow rate data from the inline flow sensor were used to exclude non-flow periods, and ship metadata (e.g., hoist position, speed) were used to flag unreliable data. Only data collected within the start and end times of sampling stations were retained.

Subsequently, a series of quality control steps were conducted on both the bulk and filtered datasets. Spectra with high relative variability were excluded, defined as a standard deviation to median ratio above certain percentile (e.g., 90th at most stations). Given the temperature differences between the Antarctic cold seawater and the warm laboratory environment where the AC-S operated, measurements collected after thermal stabilisation were used, which was assessed using the temperature recorded by the AC-S.

Spectrally anomalous data, defined as any 1-minute spectrum with more than half its values falling outside $\pm$ 1 IQR (bounded by the 16th and 84th percentiles) from the station median, were removed. This procedure was applied separately to bulk and filtered datasets. To correct for transient effects during the automatic filter switch from bulk to filtered seawater, filtered time-series of each hour were fitted to an exponential model, and the intercept derived was used as the corrected value for the 0.2 μm-filtered values for that hour. For stations with multiple filtered periods, these were interpolated before subtraction from bulk signals to derive $a_p(\lambda)$ and $c_p(\lambda)$. Spectra were then smoothed using a Savitzky-Golay filter ('savgol_filter' in Python). A correction for temperature and scattering ($b_p(\lambda) = c_p(\lambda) - a_p(\lambda)$) effects was then applied following the method described by Slade et al. (2010), which adjusts for temperature-induced biases in absorption based on near-infrared optical properties. Only spectra with non-negative values across 400–700 nm were retained. The final $a_p(\lambda)$ and $c_p(\lambda)$ for each station were calculated as

the median of all valid 1-minute spectra.

In total, 37 stations of underway optical observations, specifically, $a_p(\lambda)$, were collected during the PICCOLO cruise, which can be used to estimate Chl-a using the line-height method (Boss et al., 2007; Brewin et al., 2012), such that,

$$\text{Chl-a} = \frac{a_p(676) - (0.6 \cdot a_p(650) + 0.4 \cdot a_p(714))}{0.014}, \tag{1}$$

where 0.014 represents the chlorophyll-specific absorption coefficient for phytoplankton at 676 nm, which can vary with pigment composition and phytoplankton size (Bricaud et al., 1995).

Besides, surface water samples were collected at each station for laboratory analysis of Chl-a using an in-vitro fluorometric method (Turner Trilogy fluorometer). Specifically, 100 mL of seawater was filtered, and the filters were extracted in 10 mL of acetone and stored at -20°C for up to 24 hours. After dark equilibration at room temperature, Chl-a concentrations were determined fluorometrically, with the fluorometer calibrated against known standards.

Of the 37 stations, 32 had concurrent fluorometric and a_p-derived Chl-a data. The two estimates showed strong agreement, with a correlation of 0.970, a bias of -0.052 (indicating slight underestimation by the a_p method), and a root mean square difference (RMSD) of 0.110, all calculated in $\log_{10}$ space. To improve accuracy, the chlorophyll-specific absorption coefficient in Equation 1 was optimised using these 32 match-ups. The revised coefficient is 0.0124, which reduced the bias to 0.001 and RMSD to 0.097. This regionally tuned line-height method was then applied to a_p from all 37 stations to derive Chl-a estimates for further analysis.

S2.4 Remote sensing reflectance

This study compiled a large dataset of remote sensing reflectance ($R_{rs}(\lambda)$) with concurrent Chl-a measurements (Figure S5), combining data from a previously compilation (Sun et al., 2025) with newly collected observations.

The newly added observations include high-resolution R_{rs} measurements collected during the PICCOLO cruise, where a Satlantic HyperSAS system was deployed for quasi-continuous sampling along the cruise track. The system consists of three sensors: a zenith-facing irradiance sensor (E_s), and two radiance sensors facing the sky (L_i) and sea surface (L_t), respectively. The processing of the E_s, L_i, and L_t and the calculation of $R_{rs}(\lambda)$ followed procedures similar to those used in previous Atlantic Meridional Transect cruises (Brewin et al., 2016; Lin et al., 2022;

Pardo et al., 2023). Specifically, raw data were extracted using Satlantic SatView and SatCon software, and were dark-corrected. The three radiometric data were then synchronised to the nearest second, and only records with fully matched timestamps across all three sensors were retained.

A series of quality control filters were applied for R_{rs} measurements in the PICCOLO cruise: (1) due to the low sun elevation in the Weddell Sea during summer, solar zenith angle $\leq 80°$ to ensure adequate sun elevation; (2) an azimuth angle between 70° and 170° to reduce sun glint; (3) platform pitch and roll both within ±5° to minimise platform tilt effects; and (4) no negative radiance or irradiance values at 444 nm. To further minimise sun glint contamination, we applied a near-infrared (NIR) screening procedure based on the L_t reflectance spectrum. Only records within the lowest 10th percentile of the NIR signal were retained. R_{rs} were then calculated as, $R_{rs}(\lambda) = (L_t(\lambda) - 0.028 \cdot L_i(\lambda))/E_s(\lambda)$, where 0.028 is a standard correction factor for skylight reflection under open-ocean conditions (Mobley, 1999). To further correct for residual contamination, the average R_{rs} in the NIR band (750–800 nm) was subtracted from each spectrum. Any spectra with negative values in the visible range (400–700 nm) were discarded. Next, two spectral band ratios, $R_{rs}(443)/R_{rs}(547)$ and $R_{rs}(488)/R_{rs}(547)$, were calculated. For each ratio, the coefficient of variation (CV) was calculated, and any records with CV over 0.15 in either ratio were excluded. The median R_{rs} spectrum was then calculated for each remaining minute and used as the final quality-controlled dataset. Finally, the R_{rs} spectra were matched with underway a_p data. Only R_{rs} measurements within a ±1 hour window centred on the timestamp of each valid a_p measurement were retained. Note that during the collection of radiometry data on the PICCOLO cruise, the E_s sensor mounted on top of the central mast became contaminated by ship exhaust. To correct for this, pre- and post-cleaning data collected at the end of the cruise were used to model the relationship between E_s-derived PAR and PAR from a foremast sensor, which was less affected by exhaust. A time-dependent polynomial model was applied to correct the full E_s dataset. This correction had minimal impact on the spectral shape in the blue-green region relevant to this study.

Additional $R_{rs}(\lambda)$ from previous compilation include publicly available data from various sources, such as, BODC (Brewin et al., 2023), NASA NOMAD (NASA bio-Optical Marine Algorithm Dataset, version 2.a, Werdell and Bailey, 2005), NASA SeaWiFS Bio-optical Archive and Storage System (SeaBASS, Werdell et al., 2003), PANGAEA (Taylor et al., 2011a; Bracher, 2014, 2015d, 2017a,b; Kramer et al., 2021; Xi et al., 2021; Bracher and Cheah, 2022; Valente et al., 2022), and some published works (Brewin et al., 2023; Jordan et al., 2024). These measurements were generally obtained from radiometric observations, using instruments such as Sat-

lantic HyperSAS/Free-Falling Optical Profile, RAMSES TriOS, following the ocean optics protocols (Mueller et al., 2003) and factory user guidelines.

To ensure consistent data quality, all R_{rs} measurements with unrealistically high values (i.e., >0.15 sr^{-1}) being discarded. The dataset included both multispectral and hyperspectral observations. Any samples with fewer than six valid spectral bands were excluded. Hyperspectral data with spectral resolution of 2 nm or finer were interpolated to 1 nm. Quality assurance (QA) scores were computed following the method of Wei et al. (2016), with wavelength bands selected on a per-sample basis, and only those samples with QA scores over 0.80 were retained. Since the OCMF model does not simulate Raman scattering, corrections for Raman effects were applied to R_{rs} prior to analysis, using the approach from Lee et al. (2013). Due to the lack of detailed information about sensor mounting angles and observational geometry, bidirectional reflectance distribution function corrections were not applied.

After applying all filtering and quality control procedures, a total of 1,829 R_{rs} samples from Case-1 waters (based on water type information from OC-CCI, see Section S3.2) were retained for analysis, including 203 from the Southern Ocean and 1,626 from the tropical–subtropical regions.

S3 Auxiliary datasets

S3.1 Sea surface temperature

Sea surface temperature (SST) was obtained for each Chl-a sample to support forward modelling in the Ocean Colour Modelling Framework (OCMF), specifically for estimating temperature-dependent variables (i.e., backscattering coefficients of pure water) in two regions. SST values were sourced from the NOAA Optimum Interpolation Sea Surface Temperature (OISST) dataset, version 2, which provides global daily coverage at a 1/4° spatial resolution. This OISST dataset integrates observations from satellites, ships, buoys, and Argo floats, and is distributed by NOAA's Physical Sciences Laboratory (https://psl.noaa.gov/data/gridded/data.noaa.oisst.v2.highres.html). Each in-situ Chl-a sample was matched to the nearest OISST in space (latitude and longitude) and time (daily), and only samples with SST values between -1.8 and 40 °C were retained. Due to the limited availability of concurrent in-situ temperature data (e.g., from CTD casts), OISST match-ups were used instead. Previous study has shown high consistency between OISST and in-situ temperature measurements (see Supplementary Figure

S4 in Sun et al. (2023)).

S3.2 Water type classification

This study used monthly Ocean Colour Climate Change Initiative (OC-CCI) dataset, version 6.0, at 4 km spatial resolution (Sathyendranath et al., 2021), available at https://climate.esa.int/en/projects/ocean-colour/. The dataset includes optical water class information (Jackson et al., 2017), where 14 optical water classes are assigned to each pixel that span a gradient from clear open-ocean waters (class 1) to highly turbid coastal regions (class 14). These classifications were used to identify samples influenced by optically complex coastal waters (Sun et al., 2025). To determine the dominant water type at each sample location, 25 years of monthly OC-CCI data (1998–2022) were used. For each pixel, the mean values across all 14 classes were computed, and the class with the highest mean value was selected as the representative water type. Samples falling into classes 12, 13, or 14 were excluded from further analysis, which are likely associated with turbid coastal waters (Jackson et al., 2017).

S4 Methods

S4.1 Diagnostic pigment analyses

Phytoplankton size classes (PSCs) were estimated from the HPLC pigment data using diagnostic pigment analysis (Brewin et al., 2010; Hirata et al., 2011), which infers the fractional contribution of three size classes (pico-, nano-, and microplankton) based on the concentrations of seven diagnostic pigments. PSC fractions were calculated by applying weighting coefficients to each pigment and summing their contributions within each size class.

Previous studies have shown that these weights vary by region (Brewin et al., 2017). Therefore, in this study, region-specific weights were derived for the Southern Ocean and the tropical–subtropical oceans using in-situ datasets. The weights were determined by minimizing the difference between the in-situ measured Chl-a concentration (C) and the weighted sum of the seven diagnostic pigments (C_w), expressed as $C_W = \sum_{i=1}^{7} W_i P_i$, where P_i represents the concentration of each diagnostic pigment and W_i is its corresponding weight, with i = fucoxanthin, peridinin, 19'-hexanoyloxyfucoxanthin, 19'-butanoyloxyfucoxanthin, alloxanthin, total chlorophyll-b, and zeaxanthin. The regional weights were computed using multi-linear regression on their corresponding datasets in $\log_{10}$ space, as shown in Table S1. Using these newly

derived weights, the C_w showed strong agreement with the C, with correlation coefficients and root mean square differences ($\log_{10}$ space; see Methods in the main text) of 0.980 and 0.107 for the Southern Ocean, and 0.977 and 0.093 for the tropical–subtropical oceans, respectively.

Following Brewin et al. (2015), the fractional contributions of PSCs to total Chl-a were then calculated,

$$F_1 = \begin{cases} \frac{(-12.5C\ +\ 1)W_3P_3}{C_w}\ +\ \frac{\sum_{i=6}^{7} W_iP_i}{C_w} & \text{if } C \leq 0.08 \text{ mg m}^{-3} \\ \frac{\sum_{i=6}^{7} W_iP_i}{C_w} & \text{if } C > 0.08 \text{ mg m}^{-3} \end{cases}, \tag{2}$$

$$F_2 = \begin{cases} \frac{-12.5CW_3P_3}{C_w}\ +\ \frac{\sum_{i=4}^{5} W_iP_i\ +\ W_1P_{1,n}}{C_w} & \text{if } C \leq 0.08 \text{ mg m}^{-3} \\ \frac{\sum_{i=3}^{5} W_iP_i\ +\ W_1P_{1,n}}{C_w} & \text{if } C > 0.08 \text{ mg m}^{-3} \end{cases}, \tag{3}$$

and

$$F_3 = \frac{\sum_{i=1}^{2} W_iP_i\ -\ W_1P_{1,n}}{C_w}, \tag{4}$$

where F_1, F_2, and F_3 represent fractions of pico-, nano-, and microplankton, respectively. Since fucoxanthin can be found in both micro- and nanoplankton, a portion of this pigment was assigned to the nanoplankton group (Devred et al., 2011). This adjusted contribution, $P_{1,n}$, was computed using the expression $P_{1,n} = 10^{q_1\log_{10}(P_3)+q_2\log_{10}(P_4)}$, where P_3 and P_4 represent 19'-hexanoyloxyfucoxanthin and 19'-butanoyloxyfucoxanthin, with region-specific coefficients q_1 and q_2 derived through regression in $\log_{10}$ space (see Table S1). When $P_{1,n}$ exceeded P_1, it was capped to P_1. The Chl-a specific to each size class, pico- (C_1), nano- (C_2), micro- (C_3), and combined pico- and nanoplankton ($C_{1,2}$), were calculated by multiplying their respective fractions (Equations 2–4) by the total in-situ Chl-a concentration (C).

Table S1. Weighting coefficients for the seven diagnostic pigments and adjustment coefficients for fucoxanthin, used in this study for the Southern Ocean and the tropical–subtropical oceans. Values in brackets indicate the standard deviations associated with each weight and coefficient.

Pigments	Weights		
	W	Southern Ocean	Tropical–subtropical oceans
Fucoxanthin (P_1)	W_1	1.30 (0.01)	1.68 (0.02)
Peridinin (P_2)	W_2	0.91 (0.04)	0.87 (0.05)
19'-Hexanoyloxyfucoxanthin (P_3)	W_3	1.02 (0.01)	1.37 (0.01)
19'-Butanoyloxyfucoxanthin (P_4)	W_4	0.82 (0.03)	0.73 (0.03)
Alloxanthin (P_5)	W_5	1.60 (0.02)	4.24 (0.13)
Total chlorophyll-b (P_6)	W_6	1.31 (0.03)	0.74 (0.01)
Zeaxanthin (P_7)	W_7	1.30 (0.09)	1.07 (0.01)
Pigments	Coefficients		
	q	Southern Ocean	Tropical–subtropical oceans
19'-Hexanoyloxyfucoxanthin (P_3)	q_1	0.20 (0.03)	0.73 (0.04)
19'-Butanoyloxyfucoxanthin (P_4)	q_2	0.85 (0.02)	1.13 (0.03)

S4.2 Three-component model

Unlike previous approaches that fit the three-component model by estimating two components sequentially (i.e., fitting $F_{1,2}$ and F_1 in Equations 1 and 2 in the main text to retrieve $C^m_{1,2}$, $D_{1,2}$, C^m_1, and D_1), this study employs a multivariable least-squares optimisation approach. This approach combines residuals from multiple components into a single objective function, with each residual weighted by the inverse of its standard deviation to account for measurement uncertainty. Owing to the interdependence of model variables (size fractions), the multivariable approach offers the advantage of accounting for these interactions, resulting in more consistent parameter estimates. To ensure robust parameter estimation, we evaluated different combinations of components, such as $F_{1,2}$ with F_1, $F_{1,2}$ with F_2, and F_1 with F_2 and F_3. Across different combinations, parameter estimates and model performance were broadly consistent, with the pairing of $F_{1,2}$ and F_2 having the most accurate results.

Therefore, for the tropical–subtropical oceans, the three-component model was fitted using non-linear least-squares optimisation ('lmfit' in Python), based on in-situ C, $F_{1,2}$, and F_2. The resulting parameter estimates and their 95% confidence intervals are presented in Table S2. The relationships between Chl-a and size fractions from this study are consistent with those in

previous studies (Figure S6), reflecting overlap in data distributions (Brewin et al., 2014b; Sun et al., 2023).

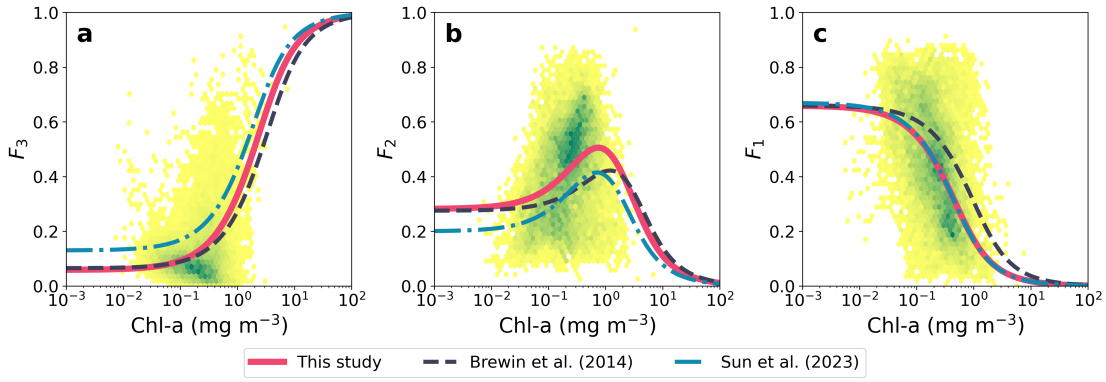

Figure S6. Fractional contributions of phytoplankton size classes, microplankton (a), nanoplankton (b), and picoplankton (c), as a function of total Chl-a in the tropical–subtropical ocean dataset. Background shading shows a density plot of the in-situ observations, with darker green indicating a higher number of data points. The re-tuned three-component model developed in this study is shown alongside model fits from previous studies (Brewin et al., 2014b; Sun et al., 2023) for comparison. The model parameters ($C^m_{1,2}$, C^m_1, $D_{1,2}$, D_1) are 1.785, 0.370, 0.935, 0.660 (see their Table ts01, Brewin et al., 2014b), and 0.95, 0.17, 0.87, 0.67 (see their Table 2, Sun et al., 2023), respectively.

In the Southern Ocean, the original exponential model struggled to capture the relationship between total Chl-a and PSCs. For example, microplankton contributions (F_3) were highly variable across the full Chl-a range, with no clear exponential trend (Figure S7a). This contrasts with the tropical–subtropical regions, where F_3 increases gradually at low Chl-a and more sharply beyond 0.3 mg m^{-3} (Figure S6a), a pattern well captured by the exponential model. However, in the Southern Ocean, F_3 values spanned the full 0–1 range even at low Chl-a, making it difficult to fit a single exponential curve across the dataset. To address this issue, we developed a modified fitting approach tailored to the distributional characteristics of the Southern Ocean dataset. The dataset was divided into quantile-based bins for Chl-a and PSCs fractions, and the median values within each bin were computed to represent major tendencies. The exponential model was then fitted to these binned median values rather than the original data points. To evaluate the influence of bin resolution on the parameter result, we conducted a sensitivity analysis by varying the number of samples per bin (step size) from 1 to 30, which effectively adjusts the number of bins. We observed that as step size increased, the values of $D_{1,2}$ and D_1 for the Southern Ocean also increased, stabilising near one when the step size exceeds 14 (not shown). Based on this trend, we selected a step size of 13 for the Southern Ocean, which provided stable parameter estimates without over-smoothing the data. The model parameters are shown in Table S2. We also applied this binning-based method to the tropical–subtropical datasets. However, the parameter values, e.g., $D_{1,2}$, were already stable across step sizes and closely aligned with the

results from the original (non-binned) method. Therefore, for the tropical–subtropical regions, we retained the original fitting approach. The regional model of the Southern Ocean captures the general trend observed in previous studies (Ward, 2015; Sun et al., 2023), particularly when regional temperature information is incorporated, reflecting the cold environment of the region. However, differences are observed in the relationship between F_3 and Chl-a (Figure S7a), which can be attributed to the different fitting methods used, with the modified version aligning more closely with in-situ measurements.

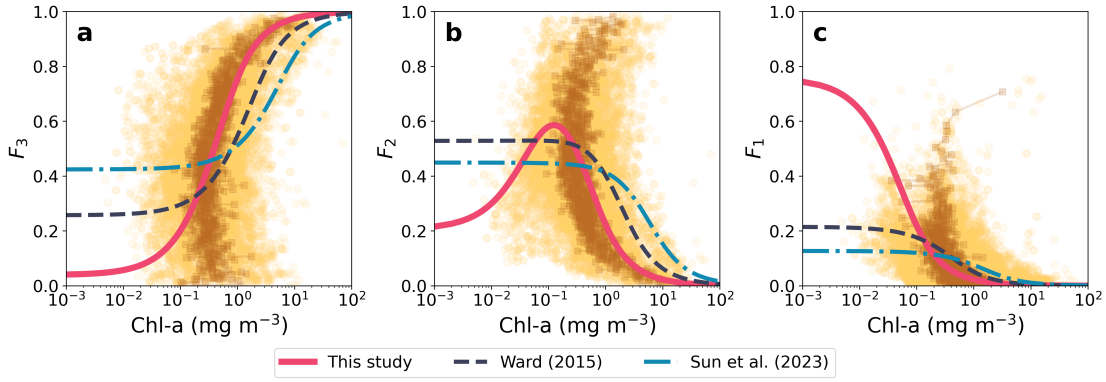

Figure S7. Fractional contributions of phytoplankton size classes, microplankton (a), nanoplankton (b), and picoplankton (c), as a function of total Chl-a in the Southern Ocean dataset (yellow circles), with quantile-binned median values shown as brown squares. The re-tuned three-component model developed in this study is shown alongside model fits from previous studies (Ward, 2015; Sun et al., 2023) for comparison. Note that model parameters here account for temperature (at 0 °C), using Equation 2 and Table 3 from Ward (2015) and Equations 8–11 and Table 2 from Sun et al. (2023), respectively.

Table S2. Parameter values of the three-component model for the Southern Ocean and tropical–subtropical regions. Values in brackets indicate the 5.55 and 94.45% confidence intervals, corresponding to two standard deviations.

Region	$C_{1,2}^m$	C_1^m	$D_{1,2}$	D_1
Southern Ocean	0.25 (0.24–0.27)	0.02 (0.02–0.02)	0.96 (0.90–1.00)	0.76 (0.43–1.00)
Tropical–subtropical oceans	1.28 (1.25–1.32)	0.17 (0.17–0.18)	0.94 (0.94–0.94)	0.66 (0.65–0.67)

References

Aiken, J., Pradhan, Y., Barlow, R., Lavender, S., Poulton, A., Holligan, P. and Hardman-Mountford, N. (2009). Phytoplankton pigments and functional types in the Atlantic Ocean: A

297 decadal assessment, 1995-2005. *Deep Sea Research Part II: Topical Studies in Oceanography*
298 56: 899–917, doi:10.1016/j.dsr2.2008.09.017.

299 Bidigare, R. R. (2012). BiG RAPA water column HPLC pigments from R/V Melville MV1015
300 in the South Pacific from Arica, Chile to Easter Island. from November to December 2010
301 (C-MORE project). Biological and Chemical Oceanography Data Management Office (BCO-
302 DMO). Version Date 2012-11-05.

303 Boss, E. S., Collier, R., Larson, G., Fennel, K. and Pegau, W. S. (2007). Measurements of spectral
304 optical properties and their relation to biogeochemical variables and processes in Crater Lake,
305 Crater Lake National Park, OR. *Hydrobiologia* 574: 149–159, doi:10.1007/s10750-006-2609-3.

306 Bracher, A. (2014). Phytoplankton pigments measured on water bottle samples during SONNE
307 cruise SO218. Alfred Wegener Institute, Helmholtz Centre for Polar and Marine Research,
308 Bremerhaven. doi:10.1594/PANGAEA.848589.

309 Bracher, A. (2015a). Phytoplankton pigment concentrations during Maria S. Merian cruise
310 MSM18/3. Alfred Wegener Institute, Helmholtz Centre for Polar and Marine Research, Bre-
311 merhaven. doi:10.1594/PANGAEA.848586.

312 Bracher, A. (2015b). Phytoplankton pigment concentrations during POLARSTERN cruise ANT-
313 XXIV/1. Alfred Wegener Institute, Helmholtz Centre for Polar and Marine Research, Bremer-
314 haven. doi:10.1594/PANGAEA.848583.

315 Bracher, A. (2015c). Phytoplankton pigment concentrations during POLARSTERN cruise ANT-
316 XXIV/4. Alfred Wegener Institute, Helmholtz Centre for Polar and Marine Research, Bremer-
317 haven. doi:10.1594/PANGAEA.848584.

318 Bracher, A. (2015d). Phytoplankton pigment concentrations during POLARSTERN cruise ANT-
319 XXVI/4. Alfred Wegener Institute, Helmholtz Centre for Polar and Marine Research, Bremer-
320 haven. doi:10.1594/PANGAEA.848585.

321 Bracher, A. (2015e). Phytoplankton pigment concentrations during POLARSTERN cruise ANT-
322 XXVII/2. Alfred Wegener Institute, Helmholtz Centre for Polar and Marine Research, Bre-
323 merhaven. doi:10.1594/PANGAEA.848590.

324 Bracher, A. (2017a). Remote sensing reflectance during POLARSTERN cruise ANT-XXV/1.
325 doi:https://doi.org/10.1594/PANGAEA.879225.

326 Bracher, A. (2017b). Remote sensing reflectance during POLARSTERN cruise ANT-XXVI/4.
327 doi:https://doi.org/10.1594/PANGAEA.879226.

Bracher, A. (2019). Phytoplankton pigment concentrations in the Southern Ocean during RV POLARSTERN cruise PS103 in Dec 2016 to Jan 2017. Alfred Wegener Institute, Helmholtz Centre for Polar and Marine Research, Bremerhaven. doi:10.1594/PANGAEA.898941.

Bracher, A. and Cheah, W. (2022). Remote sensing reflectance measured in the South China Sea and Sulu Sea during RV Sonne cruise SO218 from 18 to 27 November 2011. doi:https://doi.org/10.1594/PANGAEA.946368.

Bracher, A., Taylor, M. H., Taylor, B. B., Dinter, T., Röttgers, R. and Steinmetz, F. (2015). Phytoplankton pigment concentrations during POLARSTERN cruise ANT-XXIII/1. doi:10.1594/PANGAEA.871713.

Bracher, A., Wiegmann, S., Xi, H. and Dinter, T. (2020). Phytoplankton pigment concentration and phytoplankton groups measured on water samples obtained during POLARSTERN cruise PS113 in the Atlantic Ocean. doi:10.1594/PANGAEA.911061.

Brewin, R. J. W., Ciavatta, S., Sathyendranath, S., Jackson, T., Tilstone, G., Curran, K., Airs, R. L., Cummings, D., Brotas, V., Organelli, E., Dall'Olmo, G. and Raitsos, D. E. (2017). Uncertainty in Ocean-Color Estimates of Chlorophyll for Phytoplankton Groups. *Frontiers in Marine Science* 4, doi:https://doi.org/10.3389/fmars.2017.00104.

Brewin, R. J. W., Dall'Olmo, G., Pardo, S., Dongen-Vogels, V. van and Boss, E. S. (2016). Underway spectrophotometry along the Atlantic Meridional Transect reveals high performance in satellite chlorophyll retrievals. *Remote Sensing of Environment* 183: 82–97, doi:10.1016/j.rse.2016.05.005.

Brewin, R. J. W., Dall'Olmo, G., Sathyendranath, S. and Hardman-Mountford, N. J. (2012). Particle backscattering as a function of chlorophyll and phytoplankton size structure in the open-ocean. *Optics Express* 20: 17632, doi:10.1364/OE.20.017632.

Brewin, R. J. W., Morán, X. A. G., Raitsos, D. E., Gittings, J. A., Calleja, M. L., Viegas, M., Ansari, M. I., Al-Otaibi, N., Huete-Stauffer, T. M. and Hoteit, I. (2019). Factors Regulating the Relationship Between Total and Size-Fractionated Chlorophyll-a in Coastal Waters of the Red Sea. *Frontiers in Microbiology* 10, doi:https://doi.org/10.3389/fmicb.2019.01964.

Brewin, R. J. W., Pitarch, J., Dall'Olmo, G., Woerd, H. J. van der, Lin, J., Sun, X. and Tilstone, G. H. (2023). Evaluating historic and modern optical techniques for monitoring phytoplankton biomass in the Atlantic Ocean. *Frontiers in Marine Science* 10, doi:10.3389/fmars.2023.1111416.

Brewin, R. J. W., Sathyendranath, S., Hirata, T., Lavender, S. J., Barciela, R. M. and Hardman-Mountford, N. J. (2010). A three-component model of phytoplankton size class for the Atlantic Ocean. *Ecological Modelling* 221: 1472–1483, doi:10.1016/j.ecolmodel.2010.02.014.

Brewin, R. J. W., Sathyendranath, S., Jackson, T., Barlow, R., Brotas, V., Airs, R. and Lamont, T. (2015). Influence of light in the mixed-layer on the parameters of a three-component model of phytoplankton size class. *Remote Sensing of Environment* 168: 437–450, doi:10.1016/j.rse.2015.07.004.

Brewin, R. J. W., Sathyendranath, S., Lange, P. K. and Tilstone, G. (2014a). Comparison of two methods to derive the size-structure of natural populations of phytoplankton. *Deep Sea Research Part I: Oceanographic Research Papers* 85: 72–79, doi:https://doi.org/10.1016/j.dsr.2013.11.007.

Brewin, R. J. W., Sathyendranath, S., Tilstone, G., Lange, P. K. and Platt, T. (2014b). A multicomponent model of phytoplankton size structure. *Journal of Geophysical Research: Oceans* 119: 3478–3496, doi:10.1002/2014JC009859.

Bricaud, A., Babin, M., Morel, A. and Claustre, H. (1995). Variability in the chlorophyll-specific absorption coefficients of natural phytoplankton: Analysis and parameterization. *Journal of Geophysical Research: Oceans* 100: 13321–13332, doi:10.1029/95JC00463.

British Oceanographic Data Centre (BODC) (2020). A nutrient and carbon pump over mid-ocean ridges (RidgeMix). https://www.bodc.ac.uk/resources/inventories/cruise_inventory/report/16043/, accessed: 2025-06-26.

California Current Ecosystem LTER and Goericke, R. (2018). Size fractionation for total Chl a within the surface layer and calculated size distribution of total Chl a from discrete bottle samples from CCE-CalCOFI Augmented Cruises in the California Current System, 2004 - 2017 (ongoing). doi:10.6073/pasta/8ebed2a2ac22a27b23e7ba98f10dcbb4.

Claustre, H. (2013). Pigment concentrations in surface water during THALASSA campaign PROSOPE. doi:10.1594/PANGAEA.805388.

Claustre, H., Hooker, S. B., Heukelem, L. V., Berthon, J.-F., Barlow, R., Ras, J., Sessions, H., Targa, C., Thomas, C. S., Linde, D. van der and Marty, J.-C. (2004). An intercomparison of HPLC phytoplankton pigment methods using in situ samples: application to remote sensing and database activities. *Marine Chemistry* 85: 41–61, doi:10.1016/j.marchem.2003.09.002.

Clayton, S., Nagai, T. and Follows, M. J. (2014). (Supplement 1) Hydrochemistry and phytoplankton pigments in water samples obtained during R/V Natsushima (JAMSTEC) cruise to the Kuroshio Extension Front in October 2009. doi:10.1594/PANGAEA.819108.

Clementson, L. A. and Wojtasiewicz, B. (2019). Dataset on the absorption characteristics of extracted phytoplankton pigments. *Data in Brief* 24: 103875, doi:10.1016/j.dib.2019.103875.

Dall'Olmo, G., Westberry, T. K., Behrenfeld, M. J., Boss, E. and Slade, W. H. (2009). Significant contribution of large particles to optical backscattering in the open ocean. *Biogeosciences* 6: 947–967, doi:10.5194/bg-6-947-2009.

Devred, E., Sathyendranath, S., Stuart, V. and Platt, T. (2011). A three component classification of phytoplankton absorption spectra: Application to ocean-color data. *Remote Sensing of Environment* 115: 2255–2266, doi:10.1016/j.rse.2011.04.025.

DiTullio, G. (2011). HPLC analyses of algal pigment concentrations from the CoFeMUG cruise (KN192-05) in the South Atlantic subtropical gyre during 2007. Biological and Chemical Oceanography Data Management Office (BCO-DMO). Version Date 2011-05-18.

DiTullio, G. (2015). Sample HPLC pigments from RVIB Nathaniel B. Palmer NBP1302 cruise in the Ross Sea during 2013 (TRACERS project). Biological and Chemical Oceanography Data Management Office (BCO-DMO). Version Date 2015-05-18.

Ferreira, A., Brito, A. C., Mendes, C. R. B., Brotas, V., Costa, R. R., Guerreiro, C. V., Sá, C. and Jackson, T. (2022). OC4-SO: A New Chlorophyll-a Algorithm for the Western Antarctic Peninsula Using Multi-Sensor Satellite Data. *Remote Sensing* 14: 1052, doi:10.3390/rs14051052.

Hayward, A., Pinkerton, M. H., Wright, S. W., Gutiérrez-Rodriguez, A. and Law, C. S. (2024). Twenty-six years of phytoplankton pigments reveal a circumpolar Class Divide around the Southern Ocean. *Communications Earth & Environment* 5, doi:10.1038/s43247-024-01261-6.

Hepach, H., Quack, B., Tegtmeier, S., Engel, A., Bracher, A., Fuhlbrügge, S., Galgani, L., Atlas, E. L., Lampel, J., Frieß, U. and Krüger, K. (2016). Pigment measured on water bottle samples during METEOR cruise M91. doi:10.1594/PANGAEA.864786.

Hirata, T., Hardman-Mountford, N. J., Brewin, R. J. W., Aiken, J., Barlow, R., Suzuki, K., Isada, T., Howell, E., Hashioka, T., Noguchi-Aita, M. and Yamanaka, Y. (2011). Synoptic relationships between surface Chlorophyll-a and diagnostic pigments specific to phytoplankton functional types. *Biogeosciences* 8: 311–327, doi:10.5194/bg-8-311-2011.

IMOS (2021a). IMOS - SRS - Ocean Colour - Bio Optical Database of Australian Waters.

IMOS (2021b). IMOS National Reference Station (NRS) - Phytoplankton HPLC Pigment Composition Analysis.

Jackson, T., Sathyendranath, S. and Mélin, F. (2017). An improved optical classification scheme for the Ocean Colour Essential Climate Variable and its applications. *Remote Sensing of Environment* 203: 152–161, doi:10.1016/j.rse.2017.03.036.

Johnson, R., Strutton, P. G., Wright, S. W., McMinn, A. and Meiners, K. M. (2013). Three improved satellite chlorophyll algorithms for the Southern OceanS. *Journal of Geophysical Research: Oceans* 118: 3694–3703, doi:10.1002/jgrc.20270.

Jordan, T. M., Dall'Olmo, G., Tilstone, G., Brewin, R. J. W., Nencioli, F., Airs, R., Thomas, C. S. and Schlüter, L. (2024). A compilation of surface inherent optical properties and phytoplankton pigment concentrations from the Atlantic Meridional Transect. *Earth System Science Data* 17: 493–516, doi:10.5194/essd-17-493-2025.

Kramer, S. J., Siegel, D. A., Maritorena, S. and Catlett, D. (2021). Global surface ocean HPLC phytoplankton pigments and hyperspectral remote sensing reflectance. doi:https://doi.org/10.1594/PANGAEA.937536.

Landry, M. R. (2021). Phytoplankton HPLC pigment concentrations from samples collected in the Gulf of Mexico on R/V Nancy Foster cruises in May 2017 and May 2018. Biological and Chemical Oceanography Data Management Office (BCO-DMO) (Version 1) Version Date 2021-05-03. doi:10.26008/1912/bco-dmo.851250.1.

Lee, P. (2020). HPLC pigment data from samples collected during R/V Savannah cruises conducted in the South Atlantic Bight off the coast of Georgia from 2015-2017. Biological and Chemical Oceanography Data Management Office (BCO-DMO). (Version 1) Version Date 2020-06-19. doi:10.26008/1912/bco-dmo.816216.1.

Lee, Z., Hu, C., Shang, S., Du, K., Lewis, M., Arnone, R. and Brewin, R. (2013). Penetration of UV-visible solar radiation in the global oceans: Insights from ocean color remote sensing. *Journal of Geophysical Research: Oceans* 118: 4241–4255, doi:10.1002/jgrc.20308.

Lin, J., Dall'Olmo, G., Tilstone, G. H., Brewin, R. J. W., Vabson, V., Ansko, I., Evers-King, H., Casal, T. and Donlon, C. (2022). Derivation of uncertainty budgets for continuous above-water radiometric measurements along an Atlantic Meridional Transect. *Optics Express* 30: 45648, doi:10.1364/OE.470994.

Lohrenz, S., Chakraborty, S. and Cai, W.-J. (2020). High pressure liquid chromatography analyses of photosynthetic pigments taken on the R/V Acadian and R/V Pelican from September

452 to October 2017 in the Central northern Gulf of Mexico. Biological and Chemical Oceanog-
453 raphy Data Management Office (BCO-DMO). (Version 1) Version Date 2020-02-03. doi:
454 10.1575/1912/bco-dmo.789061.1.

455 McGillicuddy, D. (2007a). HPLC pigments, EDDIES WB cruises from R/V Weatherbird II
456 WB0409, WB0413, WB0506, WB0508 in the Sargasso Sea from 2004-2005 (EDDIES project).
457 Biological and Chemical Oceanography Data Management Office (BCO-DMO). (Version 1)
458 Version Date 2007-03-13. doi:10.1575/1912/bco-dmo.3023.1.

459 McGillicuddy, D. (2007b). Pigments from HPLC analysis of bottle samples collected during R/V
460 Oceanus cruises OC404-01, OC404-04, OC415-01 and OC415-03 from the Sargasso Sea, June
461 11, 2004 to August 24, 2005 (EDDIES project). Biological and Chemical Oceanography Data
462 Management Office (BCO-DMO). Version Date 2007-11-01. doi:10.1575/1912/5075.

463 Mobley, C. D. (1999). Estimation of the remote-sensing reflectance from above-surface measure-
464 ments. *Applied Optics* 38: 7442, doi:10.1364/AO.38.007442.

465 Mueller, J. L., Morel, A., Frouin, R., Davis, C., Arnone, R., Carder, K., Lee, Z. P., Steward,
466 R. G., Hooker, S., Mobley, C. D., McLean, S., Holben, B., Miller, M., Pietras, C., Knobel-
467 spiesse, K. D., Fargion, G. S., Porter, J. and Voss, K. (2003). *Ocean Optics Protocols For*
468 *Satellite Ocean Color Sensor Validation, Revision 4, Volume III: Radiometric Measurements*
469 *and Data Analysis Protocols*. National Aeronautical and Space administration.

470 O'Reilly, J. E. and Werdell, P. J. (2019). Chlorophyll algorithms for ocean color sensors - OC4,
471 OC5 & OC6. *Remote Sensing of Environment* 229: 32–47, doi:10.1016/j.rse.2019.04.021.

472 Palmer Station Antarctica LERT, Schofield, O., Vernet, M. and Prezelin, B. (2018). Photo-
473 synthetic pigments of water column samples and analyzed with High Performance Liquid
474 Chromatography (HPLC), collected aboard Palmer LTER annual cruises off the coast of the
475 Western Antarctica Peninsula, 1991 - 2016. doi:10.6073/pasta/4d583713667a0f52b9d2937a26d
476 0d82e.

477 Palmer Station Antarctica LTER, Schofield, O., Vernet, M. and Prezelin, B. (2020). Photosyn-
478 thetic pigments of water column samples analyzed using High Performance Liquid Chromatog-
479 raphy (HPLC), sampled during the Palmer LTER field seasons at Palmer Station, Antarctica,
480 1991 – 2015. doi:10.6073/PASTA/EC55E3D0D7260E1DF98C9156F9BECDEB.

481 Pardo, S., Tilstone, G. H., Brewin, R. J. W., Dall'Olmo, G., Lin, J., Nencioli, F., Evers-King,
482 H., Casal, T. G. D. and Donlon, C. J. (2023). Radiometric assessment of OLCI, VIIRS, and
483 MODIS using fiducial reference measurements along the Atlantic Meridional Transect. *Remote*
484 *Sensing of Environment* 299: 113844, doi:10.1016/j.rse.2023.113844.

485 Peeken, I., Bluhm, K. and Zöllner, E. (2017a). Phytoplankton pigments measured from underway
486 and water bottle samples during Marion Dufresne cruise MD158 (OOMPH MD07 leg 1). doi:
487 10.1594/PANGAEA.873203.

488 Peeken, I., Bluhm, K. and Zöllner, E. (2017b). Phytoplankton pigments measured from underway
489 and water bottle samples during Marion Dufresne cruise MD160 (OOMPH MD07 leg 2). doi:
490 10.1594/PANGAEA.873208.

491 Peeken, I., Bracher, A. and Murawski, S. (2017c). Phytoplankton pigments measured on water
492 bottle samples during POLARSTERN cruise ANT-XXIV/2. doi:10.1594/PANGAEA.873199.

493 Peeken, I. and Hoffmann, L. (2014). Phytoplankton pigments and nutrients measured on water
494 bottle samples during METEOR cruise M55. doi:10.1594/PANGAEA.869828.

495 Peeken, I. and Nachtigall, K. (2014). Pigments measured on water bottle samples during ME-
496 TEOR cruise M60. doi:10.1594/PANGAEA.869830.

497 Peeken, I. and Quack, B. (2017). Phytoplankton pigments measured on underway and water
498 bottle samples during POSEIDON cruise POS320. doi:10.1594/PANGAEA.873198.

499 Peeken, I. and Walter, S. (2017). Phytoplankton pigments measured from underway and water
500 bottle samples during POSEIDON cruise POS348. doi:10.1594/PANGAEA.873200.

501 Peeken, I., Wilken, S., Bremer, K. and Schnack-Schiel, S. B. (2017d). Phytoplankton pigments
502 measured from seawater samples from the Spermonde Archipelago in southwest Sulawesi,
503 Indonesia. doi:10.1594/PANGAEA.873209.

504 Richardson, T., Condon, R. and Neuer, S. (2013). Pigment concentrations (HPLC) from R/V
505 Atlantic Explorer cruises AE1102, AE1118, AE1206, AE1219 in the Sargasso Sea, Bermuda
506 Atlantic Time-Series Station (BATS) from 2011-2012 (Trophic BATS project). Biological and
507 Chemical Oceanography Data Management Office (BCO-DMO). (Version 1) Version Date
508 2013-06-14. doi:10.1575/1912/bco-dmo.3884.1.

509 Sathyendranath, S., Jackson, T., Brockmann, C., Brotas, V., Calton, B., Chuprin, A.,
510 Clements, O., Cipollini, P., Danne, O., Dingle, J., Donlon, C., Grant, M., Groom, S.,
511 Krasemann, H., Lavender, S., Mazeran, C., Mélin, F., Müller, D., Steinmetz, F., Valente,
512 A., Zühlke, M., Feldman, G., Franz, B., Frouin, R., Werdell, J. and Platt, T. (2021).
513 ESA Ocean Colour Climate Change Initiative (Ocean_Colour_cci): Version 5.0 Data. doi:
514 10.5285/1dbe7a109c0244aaad713e078fd3059a.

515 Slade, W. H., Boss, E., Dall'Olmo, G., Langner, M. R., Loftin, J., Behrenfeld, M. J., Roesler,
516 C. and Westberry, T. K. (2010). Underway and Moored Methods for Improving Accuracy in

Measurement of Spectral Particulate Absorption and Attenuation. *Journal of Atmospheric and Oceanic Technology* 27: 1733–1746, doi:10.1175/2010JTECHO755.1.

Sosik, H. M., Rynearson, T., Menden-Deuer, S. and OOI CGSN Data Team (2021). Size-fractionated chlorophyll from water column bottle samples collected during NES-LTER Transect cruises, ongoing since 2017. doi:10.6073/pasta/798bda0e9ddfeba20f2266e64cf4dd40.

Southern California Bight MBON, Santa Barbara Coastal LTER, Catlett, D., Siegel, D. and Guillocheau, N. (2021). Plumes and Blooms: Curated oceanographic and phytoplankton pigment observations ver 2. Environmental Data Initiative. doi:10.6073/PASTA/12BD9B9805396ECEF006549144508124.

Sun, X., Brewin, R. J. W., Sathyendranath, S., Dall'Olmo, G., Airs, R., Barlow, R., Bracher, A., Brotas, V., Kheireddine, M., Lamont, T., Marañón, E., Morán, X. A. G., Raitsos, D. E., Shen, F. and Tilstone, G. H. (2023). Coupling ecological concepts with an ocean-colour model: Phytoplankton size structure. *Remote Sensing of Environment* 285: 113415, doi:10.1016/j.rse.2022.113415.

Sun, X., Brewin, R. J. W., Sathyendranath, S., Dall'Olmo, G., Antoine, D., Barlow, R., Bracher, A., Kheireddine, M., Li, M., Raitsos, D. E., Shen, F., Tilstone, G. H. and Vellucci, V. (2025). Coupling ecological concepts with an ocean-colour model: Parameterisation and forward modelling. *Remote Sensing of Environment* 316: 114487, doi:https://doi.org/10.1016/j.rse.2024.114487.

Taylor, B. B. and Bracher, A. (2017). Pigment concentrations measured in surface water during SONNE cruise SO202/2 (TRANSBROM). doi:10.1594/PANGAEA.880235.

Taylor, B. B., Torrecilla, E., Bernhardt, A., Taylor, M. H., Peeken, I., Röttgers, R., Piera, J. and Bracher, A. (2011a). Phytoplankton pigments, composition, hyperspectral light field data and biooptical properties during POLARSTERN cruise ANT-XXV/1. doi:https://doi.org/10.1594/PANGAEA.819099.

Taylor, B. B., Torrecilla, E., Bernhardt, A., Taylor, M. H., Peeken, I., Röttgers, R., Piera, J. and Bracher, A. (2011b). Pigments of phytoplankton during POLARSTERN cruise ANT-XXV/1. doi:10.1594/PANGAEA.819070.

Uitz, J., Claustre, H., Morel, A. and Hooker, S. B. (2006). Vertical distribution of phytoplankton communities in open ocean: An assessment based on surface chlorophyll. *Journal of Geophysical Research* 111, doi:10.1029/2005JC003207.

548 Vaillancourt, R. D. and Marra, J. F. (2011). Chlorophyll derived from HPLC from R/V Atlantic
549 Explorer and R/V Cape Hatteras multiple cruises in the Sargasso Sea, Bermuda Atlantic
550 Time Series (BATS) area, and Hydrostation "S" from 2007 to 2008 (ON DEQUE project).
551 Biological and Chemical Oceanography Data Management Office (BCO-DMO). Version Date
552 2011-09-09.

553 Valente, A., Sathyendranath, S., Brotas, V., Groom, S., Grant, M., Jackson, T., Chuprin, A.,
554 Taberner, M., Airs, R., Antoine, D., Arnone, R., Balch, W. M., Barker, K., Barlow, R.,
555 Bélanger, S., Berthon, J.-F., Beşiktepe, Ş., Borsheim, Y., Bracher, A., Brando, V., Brewin,
556 R. J. W., Canuti, E., Chavez, F. P., Cianca, A., Claustre, H., Clementson, L., Crout, R.,
557 Ferreira, A., Freeman, S., Frouin, R., García-Soto, C., Gibb, S. W., Goericke, R., Gould,
558 R., Guillocheau, N., Hooker, S. B., Hu, C., Kahru, M., Kampel, M., Klein, H., Kratzer,
559 S., Kudela, R., Ledesma, J., Lohrenz, S., Loisel, H., Mannino, A., Martinez-Vicente, V.,
560 Matrai, P., McKee, D., Mitchell, B. G., Moisan, T., Montes, E., Muller-Karger, F., Neeley,
561 A., Novak, M., O'Dowd, L., Ondrusek, M., Platt, T., Poulton, A. J., Repecaud, M., Röttgers,
562 R., Schroeder, T., Smyth, T., Smythe-Wright, D., Sosik, H. M., Thomas, C., Thomas, R.,
563 Tilstone, G., Tracana, A., Twardowski, M., Vellucci, V., Voss, K., Werdell, J., Wernand, M.,
564 Wojtasiewicz, B., Wright, S. and Zibordi, G. (2022). A compilation of global bio-optical in
565 situ data for ocean colour satellite applications – version three. *Earth System Science Data*
566 14: 5737–5770, doi:10.5194/essd-14-5737-2022.

567 Venables, H., Meredith, M. P., Hendry, K. R., Hoopen, P. ten, Peat, H., Chapman, A., Beaumont,
568 J., Piper, R., Miller, A. J., Mann, P., Rossetti, H., Massey, A., Souster, T., Reeves, S.,
569 Fenton, M., Heiser, S., Pountney, S., Reed, S., Waring, Z., Clark, M., Bolton, E., Mathews,
570 R., London, H., Clement, A., Stuart, E., Reichardt, A., Brandon, M., Leng, M., Arrowsmith,
571 C., Annett, A., Henley, S. F. and Clarke, A. (2023). Sustained year-round oceanographic
572 measurements from Rothera Research Station, Antarctica, 1997–2017. *Scientific Data* 10, doi:
573 10.1038/s41597-023-02172-5.

574 Vidussi, F., Claustre, H., Manca, B. B., Luchetta, A. and Marty, J.-C. (2001). Phytoplankton
575 pigment distribution in relation to upper thermocline circulation in the eastern Mediterranean
576 Sea during winter. *Journal of Geophysical Research: Oceans* 106: 19939–19956, doi:10.1029/
577 1999JC000308.

578 Ward, B. A. (2015). Temperature-Correlated Changes in Phytoplankton Community Structure
579 Are Restricted to Polar Waters. *PLOS ONE* 10: e0135581, doi:10.1371/journal.pone.0135581.

580 Wei, J., Lee, Z. and Shang, S. (2016). A system to measure the data quality of spectral remote

sensing reflectance of aquatic environments. *Journal of Geophysical Research: Oceans* doi: 10.1002/2016JC012126.

Werdell, P. J. and Bailey, S. W. (2005). An improved in-situ bio-optical data set for ocean color algorithm development and satellite data product validation. *Remote Sensing of Environment* 98: 122–140, doi:10.1016/j.rse.2005.07.001.

Werdell, P. J., Bailey, S. W., Fargion, G. S., Pietras, C., Knobelspiesse, K. D., Feldman, G. C. and McClain, C. R. (2003). Unique data repository facilitates ocean color satellite validation. *EOS Trans. AGU* 84: 377.

Xi, H., Losa, S. N., Mangin, A., Garnesson, P., Bretagnon, M., Demaria, J., Soppa, M. A., Hembise Fanton d'Andon, O. and Bracher, A. (2021). A data set of collocated satellite remote sensing reflectance from GlobColour merged products, chlorophyll a concentration of phytoplankton functional types derived from in situ pigment data, and CMEMS sea surface temperature from 2002 to 2012. doi:https://doi.pangaea.de/10.1594/PANGAEA.930087.

Xi, H., Peeken, I., Gomes, M., Brotas, V., Tilstone, G. H., Brewin, R. J. W., Dall'Olmo, G., Tracana, A., Alvarado, L. M. A., Murawski, S., Wiegmann, S. and Bracher, A. (2023). Phytoplankton pigment concentrations and phytoplankton groups measured on water samples collected from various expeditions in the Atlantic Ocean from 71°S to 84°N. doi:10.1594/PANGAEA.954738.